

# A peptide-display protein scaffold to facilitate single molecule force studies of aggregation-prone peptides

Ciaran P. A. Doherty <sup>1,2</sup> Lydia M. Young,<sup>1,2</sup> Theodoros K. Karamanos,<sup>1,2</sup> Hugh I. Smith,<sup>1,2</sup> Matthew P. Jackson,<sup>1,2</sup> Sheena E. Radford,<sup>1,2</sup> and David J. Brockwell <sup>1,2\*</sup>

<sup>1</sup>Astbury Centre for Structural Molecular Biology, University of Leeds, Leeds LS2 9JT, United Kingdom

<sup>2</sup>School of Molecular and Cellular Biology, Faculty of Biological Sciences, University of Leeds, Leeds LS2 9JT, United Kingdom

Received 4 December 2017; Accepted 5 February 2018

DOI: 10.1002/pro.3386

Published online 00 Month 2018 proteinscience.org

**Abstract:** Protein aggregation is linked with the onset of several neurodegenerative disorders, including Parkinson's disease (PD), which is associated with the aggregation of  $\alpha$ -synuclein ( $\alpha$ Syn). The structural mechanistic details of protein aggregation, including the nature of the earliest protein-protein interactions, remain elusive. In this study, we have used single molecule force spectroscopy (SMFS) to probe the first dimerization events of the central aggregation-prone region of  $\alpha$ Syn (residues 71–82) that may initiate aggregation. This region has been shown to be necessary for the aggregation of full length  $\alpha$ Syn and is capable of forming amyloid fibrils in isolation. We demonstrate that the interaction of  $\alpha$ Syn<sub>71-82</sub> peptides can be studied using SMFS when inserted into a loop of protein L, a mechanically strong and soluble scaffold protein that acts as a display system for SMFS studies. The corresponding fragment of the homolog protein  $\gamma$ -synuclein ( $\gamma$ Syn), which has a lower aggregation propensity, has also been studied here. The results from SMFS, together with native mass spectrometry and aggregation assays, demonstrate that the dimerization propensity of  $\gamma$ Syn<sub>71-82</sub> is lower than that of  $\alpha$ Syn<sub>71-82</sub>, but that a mixed  $\alpha$ Syn<sub>71-82</sub>:  $\gamma$ Syn<sub>71-82</sub> dimer forms with a similar propensity to the  $\alpha$ Syn<sub>71-82</sub> homodimer, slowing amyloid formation. This work demonstrates the utility of a novel display method for SMFS studies of aggregation-prone peptides, which would otherwise be difficult to study.

**Keywords:** single molecule force spectroscopy; alpha-synuclein; gamma-synuclein; aggregation; amyloid; mass spectrometry

Additional Supporting Information may be found in the online version of this article.

This is an open access article under the terms of the Creative Commons Attribution License, which permits use, distribution and reproduction in any medium, provided the original work is properly cited.

Grant sponsor: European Research Council; Grant numbers: 322408, FP7.2007-2013; Grant sponsor: Biotechnology and Biological Sciences Research Council; Grant numbers: BB/E012558/1, BB/K02101X/1; Grant sponsor: Wellcome Trust; Grant number: 094232.

\*Correspondence to: David J. Brockwell, Faculty of Biological Sciences, School of Molecular and Cellular Biology, University of Leeds, Leeds LS2 9JT, United Kingdom. E-mail: d.j.brockwell@leeds.ac.uk

## Introduction

Studying protein aggregation is a significant challenge, owing to the fact that the aggregating species along the assembly pathway are often heterogeneous, transiently populated and evolve on an exponential timescale towards higher order, end point species.<sup>1–3</sup> Early events in the aggregation cascade are consequently difficult to study but are of critical importance in enhancing our fundamental understanding of the aggregation process. Gaining a greater mechanistic and structural understanding of early events in aggregation is especially important for amyloid diseases where the identity of the toxic species is still unclear.<sup>4</sup> Inhibition of early events in

the aggregation cascade are thus attractive targets for preventative and curative treatments for these diseases.

Single molecule approaches using fluorescence,<sup>5,6</sup> or force spectroscopy using either the AFM<sup>7–17</sup> or optical tweezers<sup>18</sup> are potentially powerful methods to interrogate aggregating systems as they can be performed at low concentrations, limiting aggregation, and decreasing the rate of assembly. In SMFS, monomers of the aggregation-prone species are immobilized to force sensors, separating the first protein–protein interactions from heterogeneous higher order species that complicate data analysis in other approaches. SMFS can yield information on both the strength of the interaction (and therefore off rates)<sup>19</sup> and on the location of the interaction interface via measurement of the end-to-end length of the complex at rupture.<sup>20</sup> Application of SMFS to the aggregation field, however, is challenging due to difficulties in deconvoluting nonspecific interactions from *bona fide* protein–protein interactions, both of which usually occur close to the surface.<sup>21</sup> Separation of signal from noise is especially challenging when studying small aggregation-prone proteins, such as A $\beta$ 42,<sup>22</sup> or peptide fragments from larger proteins that are thought to drive aggregation such as the nonamyloid component (NAC) region of  $\alpha$ Syn.<sup>23,24</sup> This is because these peptides can interact with inert surfaces and take part in multipartite interactions between the tip and surface. As the peptide end-to-end length is inherently short (<5 nm), these nonspecific interactions occur close to the surface. For experiments that extend a single protein (mechanical unfolding), some of these problems have been addressed by site-specific immobilization onto passivated surfaces<sup>25</sup> or by insertion of the protein of interest into a mechanically strong protein within a protein concatemer.<sup>26</sup> For protein–protein interaction studies, Lyubchenko and coworkers have developed a “flexible nanoarray” method<sup>27,28</sup> whereby pairs of aggregation-prone peptides are tethered onto an extensible linker at a defined separation, allowing dimerization events to be analyzed.<sup>27</sup> Extending the tether using the AFM allows dissociation to be measured away from the surface. While allowing measurement of dissociation, this approach requires the synthesis of bespoke polyethylene glycol-phosphoramidite linkers.<sup>21</sup> Another approach developed by Vera and Carrión-Vázquez<sup>29</sup> used a disulfide-linked polyprotein construct that allowed direct identification of single molecule dissociation events of the highly avid cohesin–dockerin complex. This method allows for internally controlled SMFS experiments on protein–protein interactions. It is, however, complex to implement, requires formation of a trimer and has not been used to analyze intermolecular interactions in a noncognate, aggregation-prone system.

In this study, we report the development and validation of a novel, easy to implement method by which an aggregation-prone region of a protein of interest is engineered into a loop of the mechanically stable monomeric carrier protein, protein L. The central NAC region (residues 71–82) of  $\alpha$ Syn (part of the wider NAC region encompassing residues 61–95) was chosen to assess this display system as this hydrophobic, 12-residue sequence (<sup>71</sup>VTGVTA-VAQKT<sup>82</sup>V) is known to be both sufficient and necessary for aggregation<sup>24</sup> and to form the core of fibrils of wild-type  $\alpha$ Syn.<sup>30</sup> We show that protein L is a suitable scaffold protein, maintaining its structure and stability after insertion of guest sequences. SMFS experiments using an AFM tip and surface derivatized with the protein L scaffold containing  $\alpha$ Syn<sub>71–82</sub> yield rupture events with correlated dissociation force and unfolding distances. By contrast, protein L constructs containing a control (GS)<sub>6</sub> linker or  $\gamma$ Syn<sub>71–82</sub> (the central NAC region derived from the less aggregation-prone  $\gamma$ Syn homolog of  $\alpha$ Syn<sup>31,32</sup>) yielded insignificant rupture events. Interestingly, an interaction is observed between  $\alpha$ Syn<sub>71–82</sub> and  $\gamma$ Syn<sub>71–82</sub> using SMFS in the pL scaffold, consistent with the postulated interaction between the full-length proteins.<sup>32</sup> We then use native electrospray ionization-ion mobility spectrometry-mass spectrometry (ESI-IMS-MS), which enables the detailed interrogation of individual species within a heterogeneous, assembling mixture,<sup>33–37</sup> to validate these results. SMFS can thus yield novel insight into the early stages of amyloid formation by insertion of aggregation-prone sequences of interest into the mechanically and thermodynamically stable scaffold, protein L.

## Results

### *Design and characterization of a protein L scaffold*

A scaffold protein should (a) allow the presentation of the amyloidogenic peptide in a defined geometry away from the surface; (b) be thermodynamically and mechanically stable after insertion of the sequence of interest, and (c) display minimal self-aggregation. The IgG binding domain of protein L [Fig. 1(A)] fulfills these criteria. This protein comprises a four stranded  $\beta$ -sheet packed against an  $\alpha$ -helix and has been shown previously to withstand the insertion of both folded and unfolded amino-acid sequences into the  $\beta$ 3– $\beta$ 4 loop<sup>39</sup> and to show mechanical resistance when extended via its termini.<sup>40</sup> The scaffold shown in Figure 1(A) is based on protein L W47Y I60F (herein termed pL), a variant rationally designed to display enhanced mechanical strength.<sup>41</sup> To ensure that the guest peptide sequence is sterically free from the pL host, the amyloidogenic peptide was inserted into the center

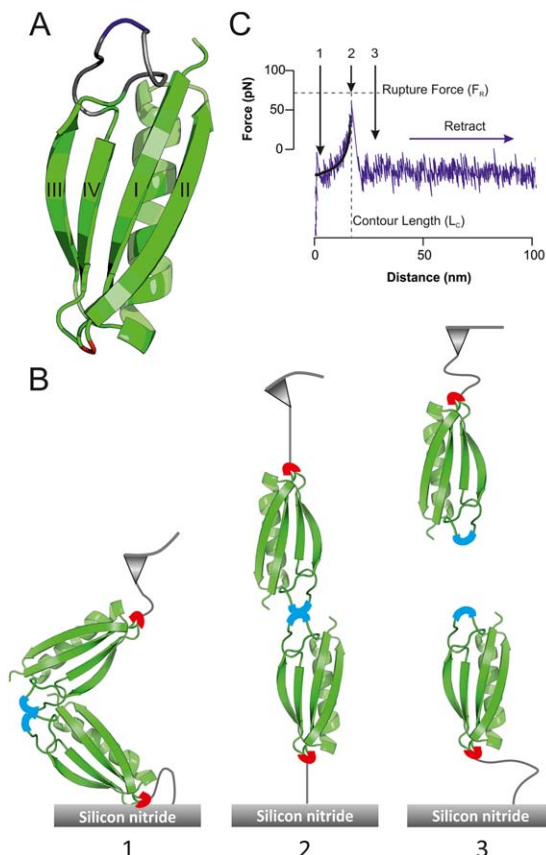


**Figure 1.** Using pL as a peptide-presenting scaffold. (A) Structural model of the pL scaffold. The  $\beta 3$ – $\beta 4$  loop, peptide insert and Cys residue for immobilization are shown in gray, blue, and red, respectively. The  $\beta 3$ – $\beta 4$  loop was extended using SWISS-MODEL and the PDB file 1HZ6.<sup>38</sup> (B) Measuring chimeric pL dimer dissociation using the AFM. The derivatized AFM tip is brought into contact with a similarly derivatized surface (1) allowing dimerization via the guest peptide. The complex is then extended by retracting the cantilever, the force generated bends the cantilever and reaches a maximum (2) at complex dissociation [rupture force ( $F_R$ )] prior to relaxation (3). (C) Typical force-extension profile of the force induced dissociation of a mechanically resistant dimer. The positions of (1) dimerization, (2) dissociation, and (3) relaxation are shown. The contour length ( $L_C$ ) and  $F_R$  are measured for each dissociation event, the former parameter obtained by fitting the Worm Like Chain (WLC) model (black curve) to the profile (Materials and Methods section).

of the  $\beta 3$ – $\beta 4$  loop that had been extended by 13 residues (generating <sup>55</sup>G...GGARGS...guest peptide...GSARGGG...<sup>56</sup>Y, Fig. S1, Supporting Information). Finally, a cysteine residue was introduced into the  $\beta 1$ – $\beta 2$  loop (N14C) distal to the graft site. This allows the specific immobilization of the scaffold onto a substrate in a geometry that presents the guest sequence to the solution. When immobilized onto the AFM tip and surface, [Fig. 1(B)] this allows dimerization which, upon extension, would shear the pL N- and C-terminal strands apart. This extension geometry has previously been shown to be

mechanically robust.<sup>40,41</sup> pL scaffolds presenting  $\alpha$ Syn<sub>71–82</sub> (Fig. S2, Supporting Information) and a 12-residue nonaggregating control sequence [(GS)<sub>6</sub>, herein named GS] were constructed and each protein expressed and purified (Fig. S3, Supporting Information, Materials and Methods section). After verification of protein identity by ESI-MS (Table SI, Supporting Information), the structural integrity of each construct was assessed by far-UV CD and fluorescence emission spectroscopy. These experiments verified that all three proteins exhibited CD-spectra consistent with a mixed  $\alpha/\beta$  topology similar to that reported for wild-type protein L<sup>42</sup> [Fig. S4(A), Supporting Information]. Similarly, fluorescence emission spectra which exhibit a red shift in their

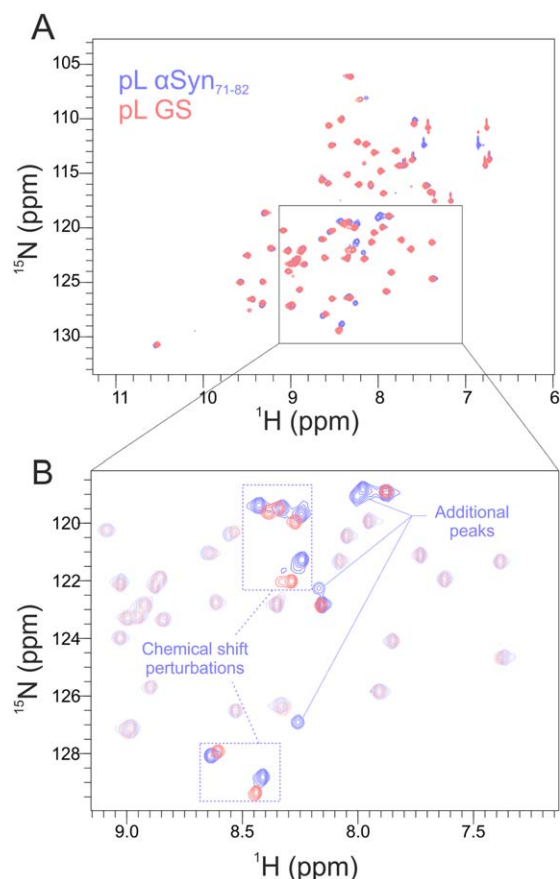


**Figure 2.** pL  $\alpha$ Syn<sub>71–82</sub> and pL GS have similar structures as revealed by HSQC NMR. The data presented shows 600 MHz <sup>1</sup>H-<sup>15</sup>N HSQC-NMR spectra of <sup>15</sup>N labeled pL  $\alpha$ Syn<sub>71–82</sub> and pL GS. (A) Overlaid spectra of pL GS (red peaks) and pL  $\alpha$ Syn<sub>71–82</sub> (blue peaks). Both spectra have dispersed and well-defined peaks characteristic of folded proteins. Additional peaks observed for pL  $\alpha$ Syn<sub>71–82</sub> at  $\sim 8$  ppm in the <sup>1</sup>H dimension most likely arise from residues in the inserted peptide in an unfolded dynamic conformation. (B) Expanded region highlighting additional peaks that are observed for pL  $\alpha$ Syn<sub>71–82</sub>. A small number of residues showing chemical shift perturbations are also highlighted (blue dashed boxes). Shifts arise because residues form part of, or are close to, the  $\beta 3$ – $\beta 4$  loop.

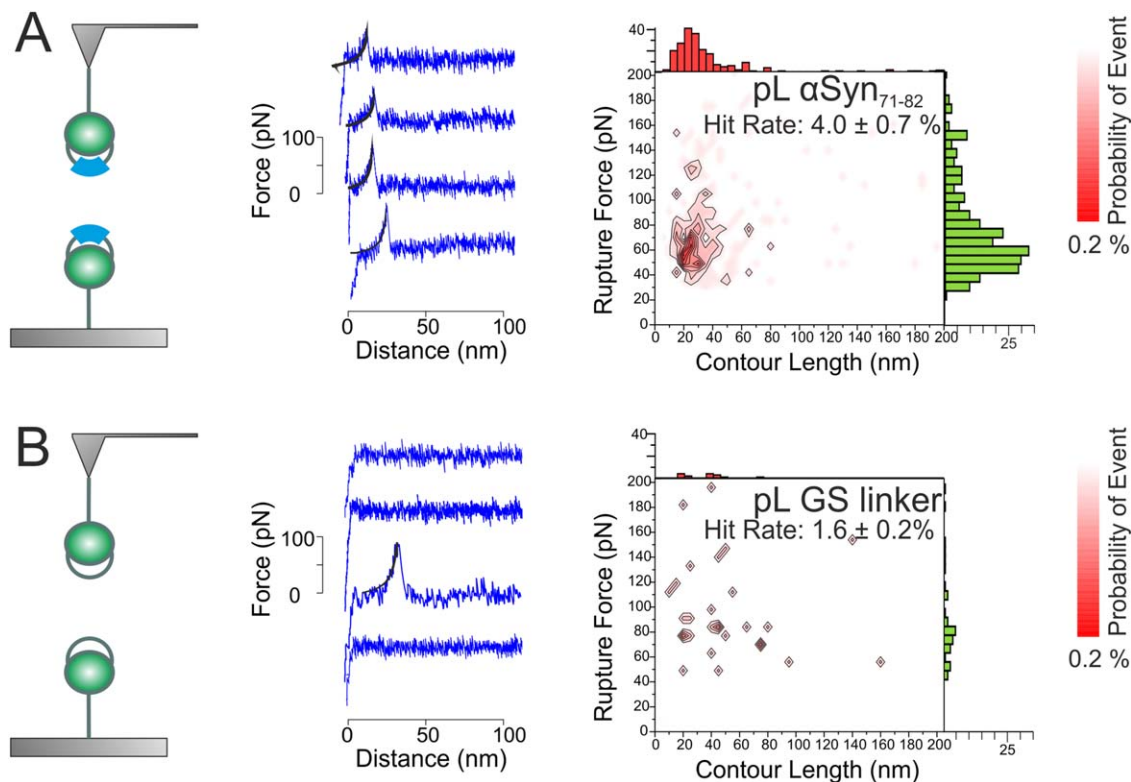


**Figure 3.** SMFS can detect dissociation events for pL  $\alpha$ Syn<sub>71-82</sub> but not pL GS. Schematic (left), sample force extension profiles (middle), and a  $F_R$  versus  $L_c$  scattergram (right, rendered as a contour plot and showing the associated  $L_c$  and  $F_R$  frequency-histograms above and to the side, respectively for (A) pL  $\alpha$ Syn<sub>71-82</sub> and (B) pL GS dissociation events). A WLC (black line) is fitted to each force-extension profile. The contour plot for pL  $\alpha$ Syn<sub>71-82</sub> shows a “hotspot” of reproducible and correlated  $L_c$  and  $F_R$  values. No “hotspot” is visible for pL GS dissociation events. The total number of force-retract cycles (total triplicate) are 8000 and 2500 for pL  $\alpha$ Syn<sub>71-82</sub> and pL GS dimerization interactions, respectively.

maxima upon denaturant-induced unfolding were observed for all proteins [Fig. S4(B), Supporting Information]. As expected for natively folded variants of protein L, thermal denaturation monitored by far-UV CD revealed co-operative unfolding transitions at a similar temperature for pL GS and pL  $\alpha$ Syn<sub>71-82</sub> [ $T_m$  values of 45.5 and 46.6°C, respectively, Fig. S4(C, D), Supporting Information].

As a more sensitive probe for structural perturbations, the  $^1\text{H}$ - $^{15}\text{N}$  heteronuclear single quantum coherence spectroscopy (HSQC) NMR spectra of pL  $\alpha$ Syn<sub>71-82</sub> and pL GS were acquired (Fig. 2). Both spectra show similarly dispersed, well defined peaks of similar intensity, characteristic of stably folded proteins [Fig. 2(A)]. Five additional main chain peaks were observed for pL  $\alpha$ Syn<sub>71-82</sub> compared with pL GS [Fig. 2(B)], likely due to the chemical shift redundancy of the glycine residues in the (GS)<sub>6</sub> linker and extended loop. Most of the additional peaks for pL  $\alpha$ Syn<sub>71-82</sub> are observed at  $^1\text{H}$  chemical shifts that are diagnostic of an unfolded protein conformation ( $\sim 8.0$  ppm), suggesting that these peaks indeed arise from unstructured  $\alpha$ Syn<sub>71-82</sub>. Overall, the CD, fluorescence, and NMR data show that grafting a 12-residue peptide sequence into the extended  $\beta$ 3- $\beta$ 4 loop does not perturb the structure

or stability of pL, validating its use as a display scaffold for SMFS experiments.

#### Dimerization of the $\alpha$ Syn central NAC region detected by SMFS

To determine whether the association of  $\alpha$ Syn<sub>71-82</sub> could be detected in the context of the protein L scaffold using AFM-based SMFS methods, the AFM probe and surface were each decorated with either pL  $\alpha$ Syn<sub>71-82</sub> or pL GS (Materials and Methods). After mounting in the AFM, force-extension profiles were accumulated. After filtering (Materials and Methods section), traces which showed a characteristic single molecule “saw tooth” profile [Fig. 1(C)] were binned for analysis. The number of these events relative to the total number of approach-retract cycles (in triplicate) was then used to calculate a ‘hit rate’ which reports on the probability of measuring the rupture (and therefore the presence) of a protein-protein interaction. As shown in Figure 1(C), for each force-extension profile, the force at rupture ( $F_R$ ) of the interaction and the end-to-end length of the dimer ( $L_c$ ) at rupture was measured. To obtain  $L_c$ , force-extension profiles were fitted to the WLC model [Materials and Methods section, Eq. (1)]. Finally, to assess whether the observed

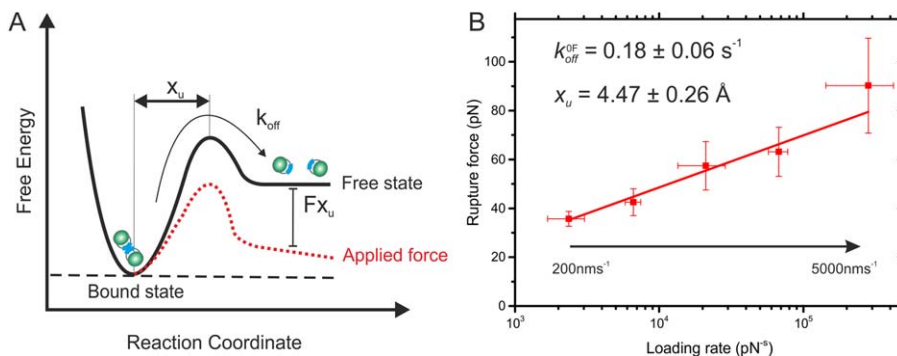


**Figure 4.** Using dynamic force spectroscopy to investigate  $\alpha\text{Syn}_{71-82}$  dissociation. (A) Schematic representation of an unbinding energy landscape. The dotted line depicts the tilted energy landscape under force.  $x_U$  is depicted as the distance from the bound energy well to the transition state.  $k_{\text{off}}^{0F}$  is shown as the stochastic process of crossing the transition energy barrier. (B) Dynamic force spectrum of  $\alpha\text{Syn}_{71-82}$  dissociation. Data (mean of the triplicate datasets, error bars are the standard deviation) are fitted to the Bell-Evans model<sup>45,46</sup> to obtain values  $k_{\text{off}}^{0F}$  and  $x_U$  (shown inset). The errors for  $k_{\text{off}}^{0F}$  and  $x_U$  were calculated by manual bootstrapping. The total number of approach retract cycles (total triplicate) for pL  $\alpha\text{Syn}_{71-82}$  dimer dissociation events are 5200, 5500, 6500, 6000, and 5500 for pulling speeds 200, 500, 1000, 3000, and 5000  $\text{nms}^{-1}$ , respectively.

dissociation events produced reproducible and correlated values of  $L_C$  and  $F_R$ , contour plots were generated (Fig. 3).

Comparison of the force-extension profiles and contour plots obtained for pL  $\alpha\text{Syn}_{71-82}$  and pL GS [Fig. 3(A, B)] revealed that the dissociation of pL  $\alpha\text{Syn}_{71-82}$ , but not pL GS, can be detected and quantified using SMFS. Force-extension profiles for pL  $\alpha\text{Syn}_{71-82}$  typically produced a single sawtooth [Fig. 3(A)], as expected for an extensible chain<sup>43</sup> with correlated  $F_R$  and  $L_C$  values ( $57 \pm 1$  pN and  $22 \pm 1$  nm, respectively) and a hit-rate of  $4.0 \pm 0.7\%$ . By contrast, force-extension profiles for pL GS were generally featureless [Fig. 3(B)]. For this protein, the frequency of binned events was lower ( $1.6 \pm 0.2\%$ ) with no ‘hotspot’ (diagnostic of a specific interaction) in the contour plot. These data indicate that SMFS can detect intermolecular interactions between amyloidogenic peptides. The modal rupture force is surprisingly large given the expected transient nature and the relatively small interaction surface of the 12-residue  $\alpha\text{Syn}$  peptide ( $F_R = 57$  pN, at a retraction velocity of  $1000 \text{ nms}^{-1}$ ). The  $F_R$  measured here is, however, similar to that measured for full length  $\alpha\text{Syn}$ <sup>14,16,17</sup> and other protein–protein interactions mediated by short peptide sequences.<sup>44</sup>

#### Dynamic force spectroscopy of the $\alpha\text{Syn}$ Central NAC region

Despite the small size of the peptide fragment  $\alpha\text{Syn}_{71-82}$  under study here, the data demonstrate that interaction between these sequences is sufficiently strong to be detected by SMFS. In order to characterize this dimer interaction further, dynamic force spectroscopy (DFS) was carried out allowing parameters of the unbinding energy landscape to be calculated [Fig. 4(A)]. The SMFS experiments were carried out at pulling velocities ranging from 200 to

$5000 \text{ nms}^{-1}$  [Fig. 4(B)]. After calculation of the loading rate at rupture [Materials and Methods section Eq. (2)], the dissociation rate constant in the absence of force ( $k_{\text{off}}^{0F}$ ) and the ‘distance’ between the dissociation energy barrier and the bound ground state ( $x_U$ ) was calculated using the Bell-Evans model<sup>45,46</sup> [Materials and Methods section, Eq. (3)]. The dissociation rate constant for pL  $\alpha\text{Syn}_{71-82}$  dimers ( $k_{\text{off}}^{0F} = 0.18 \text{ s}^{-1}$ , lifetime  $\sim 6$  s) is comparable to the dissociation rate constant of full length  $\alpha\text{Syn}$  ( $0.25 \text{ s}^{-1}$  at pH 2.7 and  $0.74 \text{ s}^{-1}$  at pH 3.7 measured by SMFS).<sup>9</sup> The finding that the lifetimes of dimers of full-length  $\alpha\text{Syn}$  and  $\alpha\text{Syn}_{71-82}$  dimers are of comparable magnitude suggests that residues 71–82 play a key role in the stability of dimeric species formed from the intact protein.

#### SMFS identifies a novel interaction between $\alpha\text{Syn}_{71-82}$ and its homolog $\gamma\text{Syn}_{71-82}$

While the presence or absence of SMFS rupture peaks for dimers of pL  $\alpha\text{Syn}_{71-82}$  and pL GS, respectively suggests that the former protein self-interacts, it does not report on the specificity of this interaction. To address this question, we inserted the central NAC domain of another member of the synuclein family,  $\gamma\text{Syn}$ , into the pL scaffold. The central NAC sequences of  $\alpha$ - and  $\gamma$ -Syn differ at five positions ( $\alpha\text{Syn}$ : <sup>71</sup>VTGVTAVAQKTV<sub>82</sub> and  $\gamma\text{Syn}$ : <sup>71</sup>VSSVNTVATKTV<sub>82</sub>) and these differences (Fig. S2, Supporting Information) may play a role in the greater amyloidogenic propensity observed for  $\alpha\text{Syn}$ .<sup>31,32</sup>

After construction, purification and characterization of pL  $\gamma\text{Syn}_{71-82}$  (Figs. S3, S4, Table SI, Supporting Information), SMFS was used to probe homodimeric (pL  $\gamma\text{Syn}_{71-82}$  on the AFM tip and surface) and heterodimeric (pL  $\gamma\text{Syn}_{71-82}$  on the AFM tip and pL  $\alpha\text{Syn}_{71-82}$  on surface) dissociation events.

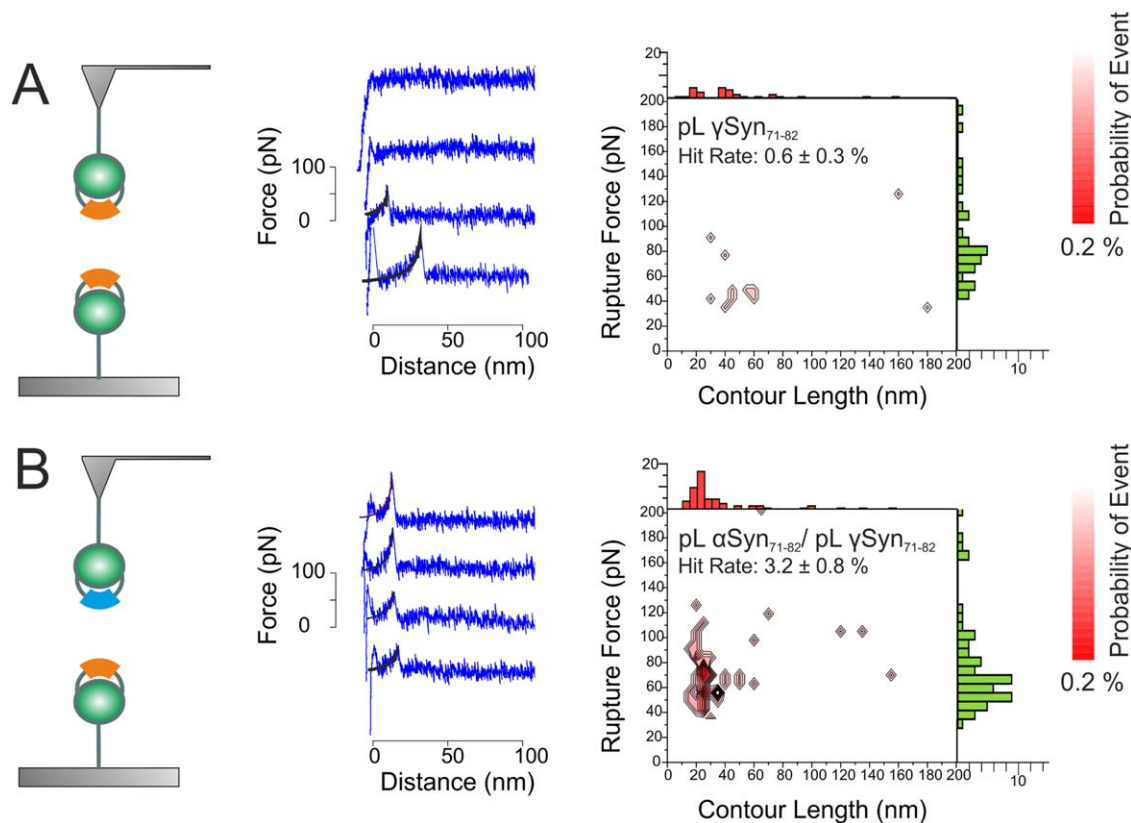


**Figure 5.** SMFS can detect dissociation events for pL  $\alpha$ Syn<sub>71-82</sub>: pL  $\gamma$ Syn<sub>71-82</sub> heterodimers but not pL  $\gamma$ Syn<sub>71-82</sub> homodimers. Schematic (left), sample force extension profiles (middle) and a  $F_R$  versus  $L_C$  contour plot (right), showing the associated  $L_C$  and  $F_R$  frequency-histograms above and to the side, respectively for (A) pL  $\gamma$ Syn<sub>71-82</sub> homodimer dissociation events and (B) pL  $\alpha$ Syn<sub>71-82</sub>:pL  $\gamma$ Syn<sub>71-82</sub> heterodimer dissociation events. WLC fits (black line) are fit for force extension profiles. While no “hotspot” is visible for the dissociation of pL  $\gamma$ Syn<sub>71-82</sub> homodimers, the contour plot for dissociation of the heterodimer shows a “hotspot” of reproducible and correlated  $L_C$  and  $F_R$  values. The modal  $L_C$  and  $F_R$  were calculated to be  $19 \pm 1$  nm and  $53 \pm 1$  pN, respectively. The total number of approach retract cycles (total triplicate) for pL  $\gamma$ Syn<sub>71-82</sub> homodimerization and  $\alpha$ Syn<sub>71-82</sub>/ $\gamma$ Syn<sub>71-82</sub> heterodimerization interactions are both 2500.

Surprisingly, the force-extension profiles and contour plots for putative homodimeric pL  $\gamma$ Syn<sub>71-82</sub> dissociation [Fig. 5(A)] show no evidence for formation of a force-resistant structure (hit rate =  $0.6 \pm 0.3\%$ , no ‘hot spot’ evident). By contrast, the dissociation of pL  $\gamma$ Syn<sub>71-82</sub>:pL  $\alpha$ Syn<sub>71-82</sub> heterodimers was readily detected using SMFS yielding comparable  $L_C$  and  $F_R$  values ( $19 \pm 1$  nm and  $53 \pm 1$  pN, respectively) to that of the  $\alpha$ Syn<sub>71-82</sub> homodimeric interaction, albeit at a lower frequency of detection ( $3.2 \pm 0.8\%$ ). Importantly, the possibility that these observations arise from differences in immobilization efficiencies between each scaffold was ruled out by sequential experiments that used the same derivatized tip but different substrates (Fig. S5, Supporting Information). The results thus portray the first observation of a heterodimeric interaction in an aggregating system by SMFS and also the first observation that the central NAC region of  $\alpha$ Syn is sufficient to interact with the corresponding sequence of its homolog  $\gamma$ Syn. Uversky *et al.* have shown previously that full length  $\alpha$ Syn fibrillation is inhibited by the presence of  $\gamma$ Syn.<sup>32</sup> One possible interpretation is that this

inhibitory effect is mediated by the interaction between the central NAC regions of these proteins.

#### Native mass spectrometry of pL constructs

SMFS shows that the central NAC regions of  $\alpha$ - and  $\gamma$ Syn are able to dimerize and be of sufficient kinetic stability to measure their dissociation using force spectroscopy. To verify this observation, ESI-MS was used as an orthogonal method to detect dimerization. This soft ionization method enables preservation of noncovalent interactions in the gas phase and allows resolution of heterogeneous species that differ in mass or charge state and, when coupled to ion mobility spectrometry (ESI-IMS-MS), cross-sectional area.<sup>47</sup> These experiments were performed using  $100 \mu\text{M}$  pL constructs in  $100 \text{ mM}$  ammonium acetate pH 6.8, and to measure formation of heterodimers, equal volumes of each sample were mixed. ESI-MS data were then accumulated immediately ( $t = 0$ ) or after quiescent incubation for 4 h at  $25^\circ\text{C}$ . Comparison of the ESI mass spectra for pL GS, pL  $\alpha$ Syn<sub>71-82</sub>, pL  $\gamma$ Syn<sub>71-82</sub>, and 1:1 pL  $\alpha$ Syn<sub>71-82</sub>:pL  $\gamma$ Syn<sub>71-82</sub> showed that all pL constructs were

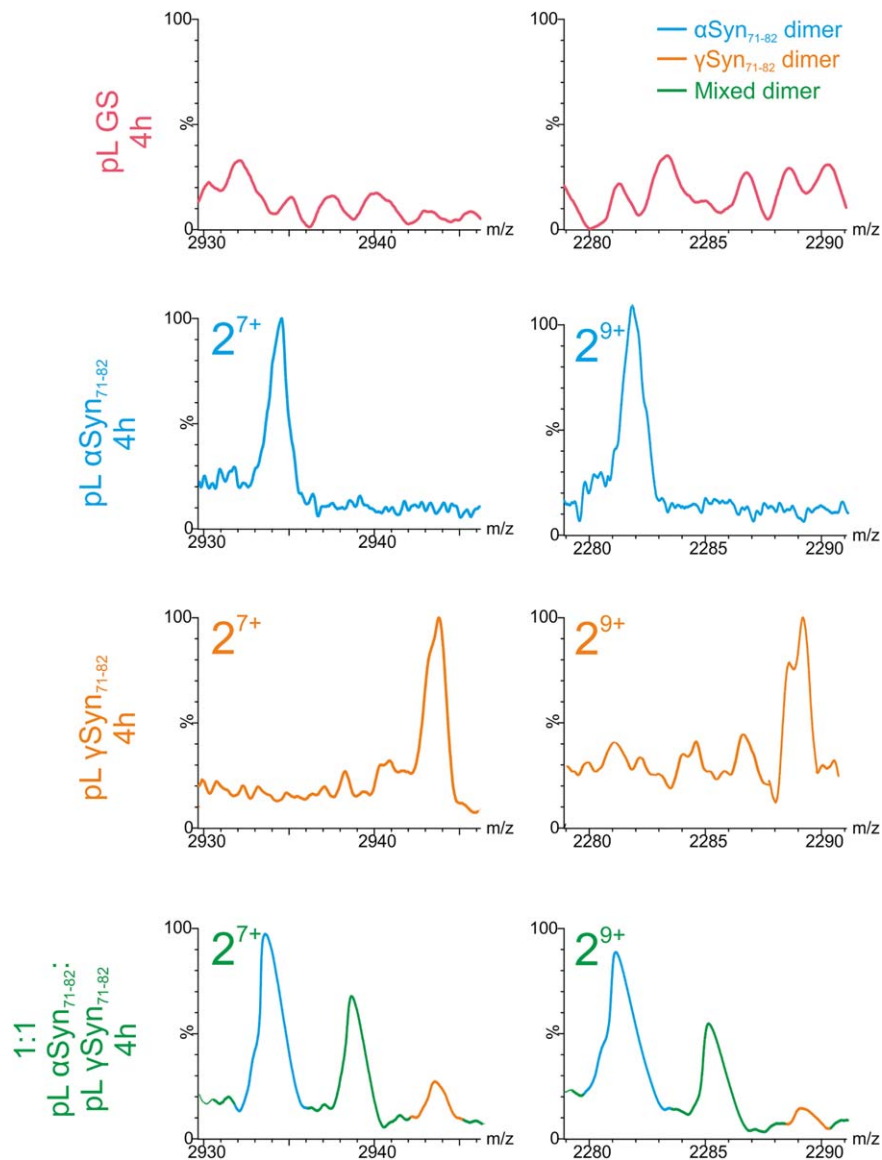


**Figure 6.** Dimeric species of chimeric pL constructs analyzed by ESI-MS. ESI-mass spectra showing two different charge states (7+ and 9+) of the dimeric species formed after 4 h incubation of pL GS (pink), pL  $\alpha$ Syn<sub>71-82</sub> (blue), pL  $\gamma$ Syn<sub>71-82</sub> (orange), and 1:1 pL  $\alpha$ Syn<sub>71-82</sub> and pL  $\gamma$ Syn<sub>71-82</sub> (heterodimer colored green). The numbers denote the oligomer order, with the positive-charge state of ions in superscript. The spectra of pL GS shows the absence of dimer after 4 h. The difference in mass between pL  $\alpha$ Syn<sub>71-82</sub> and pL  $\gamma$ Syn<sub>71-82</sub> allows pL  $\alpha$ Syn<sub>71-82</sub> and pL  $\gamma$ Syn<sub>71-82</sub> homodimers and heterodimeric species to be readily discerned from one another.

initially monomeric upon dilution ( $t = 0$ , Fig. S6, Supporting Information). In accord with the SMFS experiments described above, pL GS remained monomeric after incubation. In contrast, dimers, in addition to monomers, were observed for pL  $\gamma$ Syn<sub>71-82</sub> alone, with monomers–trimers present for pL  $\alpha$ Syn<sub>71-82</sub> and for mixtures of 1:1 pL  $\alpha$ Syn<sub>71-82</sub>:pL  $\gamma$ Syn<sub>71-82</sub> (Fig. S6, Supporting Information). For each charge state of the heterodimeric species, the difference in the molecular masses of pL  $\alpha$ Syn<sub>71-82</sub> and pL  $\gamma$ Syn<sub>71-82</sub> (10,391 and 10,423 Da, respectively) is sufficient to resolve three peaks representing homodimers of pL  $\alpha$ Syn<sub>71-82</sub> and pL  $\gamma$ Syn<sub>71-82</sub> (at  $m/z$  values for the 9+ charge state centered on  $\sim$ 2282 and 2289, Fig. 6) and a heterodimer ( $m/z$  centered on

$\sim$ 2285) corroborating the observation of a heterodimer in SMFS experiments. Interestingly, despite mixing an equal concentration of each variant, the relative intensity of each dimer species differs and mirrors the hit rate observed by SMFS experiments (from highest to lowest apparent dimer population:  $\alpha\alpha > \alpha\gamma > \gamma\gamma$ ). In the mixed samples, peaks from monomeric proteins (Fig. S6, Supporting Information) were of similar intensities, suggesting that the two peptides ionize with similar efficiency. This observation suggests that the intensities of dimer peaks indeed reflect the relative affinity of the different dimeric species.

To preclude the possibility that the interactions observed by SMFS and ESI-MS arise from the pL scaffold, the ESI-MS experiments were repeated

using  $\alpha\text{Syn}_{71-82}$  and  $\gamma\text{Syn}_{71-82}$  as synthetic peptides. ESI-IMS-MS driftscope plots of the peptides alone and in a 1:1 mixture showed the presence of monomeric to tetradecameric species (Fig. S7, Supporting Information). The higher order of species observed for the peptide-only variants suggests that packing restraints of the scaffold disfavors larger oligomer formation. Despite these differences, homodimers and heterodimers were formed upon mixing equimolar  $\alpha\text{Syn}_{71-82}:\gamma\text{Syn}_{71-82}$ , confirming that  $\alpha\text{Syn}_{71-82}$  and  $\gamma\text{Syn}_{71-82}$  sequences interact independently of the pL scaffold.

### Characterizing the aggregation of pL constructs

We have shown that the central NAC regions of  $\alpha\text{Syn}$  and  $\gamma\text{Syn}$  are sufficient to allow the formation of transient homo- and hetero-dimers and that this interaction is preserved when these short sequences are inserted into the pL scaffold. To investigate whether these pL-peptide chimeras are able to form amyloid fibrils, we examined the amyloid growth kinetics of pL  $\alpha\text{Syn}_{71-82}$  and pL  $\gamma\text{Syn}_{71-82}$  using thioflavin T (ThT) fluorescence (Fig. 7). In addition, as full length  $\gamma\text{Syn}$  has previously been shown to inhibit the kinetics of  $\alpha\text{Syn}$  aggregation,<sup>32</sup> we also measured the amyloid growth kinetics of a 1:1 mixture of pL  $\alpha\text{Syn}_{71-82}$  and pL  $\gamma\text{Syn}_{71-82}$  to test whether this inhibitory interaction was mediated by the central NAC region. The end point of ThT fluorescence emission intensity was similar for both pL  $\alpha\text{Syn}_{71-82}$  and pL  $\gamma\text{Syn}_{71-82}$  ( $785 \pm 122$  and  $929 \pm 83$  arbitrary units, respectively after 100 h) while the mixed sample appeared unable to aggregate as studied by this assay (Fig. 7). pL GS did not aggregate into ThT-positive species. Similar experiments performed on the synthetic peptides also showed that a 1:1 mixture of  $\alpha\text{Syn}_{71-82}$  and  $\gamma\text{Syn}_{71-82}$  resulted in a significant increase in lag-time [ $2.5\times$  and  $5.7\times$  increase when compared with  $\alpha\text{Syn}_{71-82}$  and  $\gamma\text{Syn}_{71-82}$  alone, respectively (Fig. S8, Supporting Information)]. These data suggest that the heterodimeric interaction identified by SMFS and ESI-MS inhibits aggregation. This supports the finding that the inhibitory effect reported for full length  $\gamma\text{Syn}$  on the aggregation of  $\alpha\text{Syn}$  is mediated by the interaction between their central NAC regions. It is important to note however, that the SMFS and ESI-MS experiments were carried out in different buffer conditions due to the buffer limitations in ESI-MS experiments. It is widely recognized that ionic strength and pH affect the rates and the dominating mechanisms in amyloid formation.<sup>48-50</sup> The inhibitory effect that  $\gamma\text{Syn}_{71-82}$  exerts on  $\alpha\text{Syn}_{71-82}$  was, however, also observed in aggregation assays performed in ESI-MS buffer conditions (Fig. S9, Supporting Information).

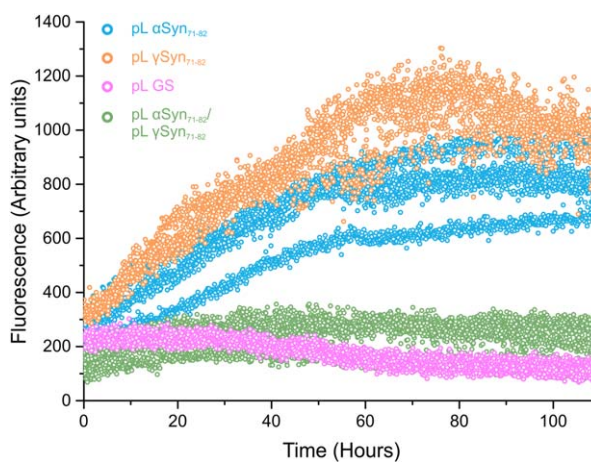


**Figure 7.** ThT fibril formation assays show that pL  $\alpha\text{Syn}_{71-82}$  inhibits the aggregation of pL  $\gamma\text{Syn}_{71-82}$ . ThT fluorescence assay showing the normalized fluorescence over time of pL  $\alpha\text{Syn}_{71-82}$  (blue), pL  $\gamma\text{Syn}_{71-82}$  (orange), pL GS (pink), and the 1:1 mix of pL  $\alpha\text{Syn}_{71-82}$  and pL  $\gamma\text{Syn}_{71-82}$  (green). Proteins were incubated at  $37^\circ\text{C}$ , 600 rpm at a final concentration of  $100 \mu\text{M}$  ( $\alpha/\gamma$  mix at  $50 \mu\text{M}$  of each protein).

### Discussion

In this study we describe the generation, characterization and proof-of-concept of a novel approach to facilitate the investigation of interactions between amyloidogenic peptides using SMFS. Using protein L as a display system, we were able to interrogate the specific interactions between synuclein sequences and to minimize the contributions of nonspecific events that often occur at the surface-proximal regions of force-distance curves.<sup>51</sup> Our approach also restricts the application of force to a defined geometry, giving more confidence that specific dimer interactions are being interrogated in a consistent manner.

Importantly, we have shown that protein L maintains sufficient stability upon insertion of amyloidogenic sequences to fold to a native state. This is significant as the ability of chimeric pL constructs to fold to a native state is integral to the ability to display peptide sequences to reduce nonspecific tip-surface interactions.

Whilst the aim of this study was to assess the potential of a scaffold display for SMFS experiments, the study has also yielded intriguing observations on the dimerization between  $\alpha\text{Syn}$  and its less aggregation-prone homolog  $\gamma\text{Syn}$ , by both SMFS and native ESI-mass spectrometry. First, DFS of the dissociation of pL  $\alpha\text{Syn}_{71-82}$  dimers revealed a lifetime that is similar to that of full length  $\alpha\text{Syn}$  (6 and 4 s for pL  $\alpha\text{Syn}_{71-82}$  and full length  $\alpha\text{Syn}$ , respectively) measured using the same technique.<sup>9</sup> It is important to note, however, that previous SMFS experiments on full-length  $\alpha\text{Syn}$  were conducted at acidic pH where the full length protein is closer to its pI and therefore more prone to aggregation.<sup>7,9,12,14,16,17</sup> The

experiments carried out here were conducted at a more physiological pH (pH 7.5) and are therefore more applicable to the conditions in which the protein self-associates *in vivo*.

To investigate the specificity of the dimer interaction, the dissociation of pL  $\gamma$ Syn<sub>71-82</sub> homodimers and pL  $\alpha$ Syn<sub>71-82</sub>:pL  $\gamma$ Syn<sub>71-82</sub> heterodimers was also investigated by SMFS. Surprisingly, no reproducible correlation between  $F_R-L_c$  values was found for pL  $\gamma$ Syn<sub>71-82</sub> homodimers, suggesting that under the conditions used, dimerization did not occur or that these dimers dissociated more quickly or at a force that cannot be detected in this experiment. By contrast, dissociation of the  $\alpha$ Syn<sub>71-82</sub>: $\gamma$ Syn<sub>71-82</sub> heterodimer yielded AFM data that were similar to those obtained for pL  $\alpha$ Syn<sub>71-82</sub> homodimers. Despite this similarity, a population of pL  $\alpha$ Syn<sub>71-82</sub>:pL  $\gamma$ Syn<sub>71-82</sub> dimers inhibits aggregation in the context of both chimeric pL constructs and synthetic peptides equivalent to the central NAC region in isolation. This suggests that the mechanism by which full length  $\gamma$ Syn inhibits the aggregation of  $\alpha$ Syn<sup>32</sup> may be mediated by the central NAC region of the proteins. As both  $\alpha$ Syn and  $\gamma$ Syn are highly expressed in many of the same cells of the brain,<sup>52</sup> it may be postulated that heterogeneous  $\alpha$ Syn and  $\gamma$ Syn dimers occur *in vivo*, which may chaperone  $\alpha$ Syn away from aggregation under normal cellular conditions. The importance of this region to the aggregation of  $\alpha$ Syn has been highlighted in a recent study,<sup>53</sup> which shows that  $\alpha$ Syn<sub>71-82</sub> derived peptides bind full-length  $\alpha$ Syn, and that modified peptides can increase its aggregation.

Together these observations provide further support for the central role of the NAC sequence in the aggregation of full length  $\alpha$ Syn. The ability of  $\beta$ Syn to inhibit the aggregation of  $\alpha$ Syn, challenges this notion, as this homolog has no NAC region but forms transient interactions with  $\alpha$ Syn up- and down-stream from the NAC sequence.<sup>32,54</sup> It is becoming clear that this intrinsically disordered protein displays conformational plasticity and that long range intra- and inter-chain interactions between the termini of this protein, which can be disrupted by changes in pH or mutation, may modulate the interaction potential of NAC.<sup>55-57</sup> The development of a facile method that will allow the relative frequency and dissociation rate of these, and other interactions, such as that reported here, may help to understand the early events in the etiology of  $\alpha$ Syn aggregation relevant to Parkinson's disease.

## Materials and Methods

### Expression and purification of pL constructs

pL constructs (Fig. S1, Supporting Information) encoded on pET23a plasmids were expressed in *Escherichia coli* BL21 (DE3) cells. Briefly, overnight starter cultures were used to inoculate 10 × 1 L LB medium supplemented with 100  $\mu$ g/mL ampicillin

and grown to an optical density at 600 nm = 0.6. Protein expression was then induced by addition of IPTG to a final concentration of 1 mM. The cultures were allowed to grow for a further 4 h before harvesting. Cell pellets were resuspended in lysis buffer [20 mM Tris.HCl pH 8.0, 300 mM NaCl, 20 mM imidazole, 2 mM DTT, 0.025% (w/v) sodium azide, 1 mM PMSF, 2 mM benzamidine, 0.15% (v/v) Triton X100, 20  $\mu$ g/mL DNase, and 100  $\mu$ g/mL lysozyme], homogenized and further lysed by cell disruption at 30 K PSI. Cell debris was removed by centrifugation at 18,000g for 30 min. The proteins were purified by affinity chromatography using a 5 mL His-Trap FF column (GE Healthcare) equilibrated with lysis buffer (without Triton X100, DNase, and lysozyme) and eluted by a stepped gradient (25, 50, and 100%) of 20 mM Tris.HCl pH 8.0, 300 mM NaCl, 250 mM imidazole, 2 mM DTT, 0.025% (w/v) sodium azide, 1 mM PMSF, 2 mM benzamidine. pL complexes were further purified using size exclusion chromatography (HiLoad™ 26/60 Superdex 75 prep grade column, GE Healthcare) equilibrated with 25 mM Tris.HCl, 300 mM NaCl, 2 mM DTT, pH 8. The protein was then dialyzed into 20 mM HEPES, pH 7.5 (for pL SMFS experiments) and flash frozen with liquid N<sub>2</sub>. The presence, purity and the correct mass of proteins were confirmed by ESI-MS.

### Thioflavin T (ThT) aggregation assays

One hundred micromolar pL constructs (in 20 mM HEPES, 20  $\mu$ M ThT, pH 7.5) were incubated at 37°C shaking at 600 rpm in a BMG Labtech FLUOstar optima plate reader in Corning 96-well flat bottom assay plates. Plates were sealed with StarSeal advanced polyolefin film (Starlab, Hamburg, Germany). To monitor growth kinetics, samples were excited at 444 nm and the fluorescence emission was monitored at 480 nm with a gain of 1450. Data were accumulated every 6.67 min over a period of >100 h.

### Synuclein peptides and Thioflavin T (ThT) fluorescence

$\alpha$ Syn<sub>71-82</sub> and  $\gamma$ Syn<sub>71-82</sub> peptides were purchased from Genscript, NJ at >99% purity. All peptides were N-terminally acetylated and C-terminally amidated. Peptides were dissolved in 100% (v/v) HFIP (hexafluoroisopropanol) at 450  $\mu$ M and dispensed into Corning 96-well flat bottom assay plates. Fifty microliter was dispensed into wells, and the HFIP was left to evaporate. The dry peptide in the well was dissolved into 100  $\mu$ L 20 mM HEPES, 20  $\mu$ M ThT, pH 7.5 to give a concentration of 225  $\mu$ M peptide. Incubations were carried out at 37°C shaking at 600 rpm. Plates were sealed with StarSeal advanced polyolefin film from Starlab, Hamburg, Germany. The fluorescence of the samples were excited at 444 nm and the fluorescence emission was monitored at 480 nm on a BMG Labtech FLUOstar

optima plate reader with a gain set at 1450. Where normalized data is presented, it has been processed on the plate reader software and normalized (after buffer subtraction) between 0 and 100. Lag time analysis was carried out by manually fitting a linear regression of the steepest exponential region of the ThT curves on Origin Pro 9.1 software. The fit was extrapolated to calculate the x-intercept (quoted lag times).

### **<sup>1</sup>H-<sup>15</sup>N HSQC NMR spectroscopy**

<sup>1</sup>H-<sup>15</sup>N HSQC spectra of 400 μM pL αSyn<sub>71-82</sub> and pL γSyn<sub>71-82</sub> (20 mM HEPES buffer, 10% (v/v) D<sub>2</sub>O and 0.02% (w/v) sodium azide, pH 7.5) were recorded on an AVANCE III Bruker spectrometer (600 MHz) equipped with a cryogenic probe. Spectra were processed in NMRPipe and analyzed in CCPN analysis.

### **Negative stain transmission electron microscopy (TEM)**

Protein samples were pipetted onto the surface of carbon coated copper grids and stained with 1% (w/v) uranyl acetate. Images were taken on an FEI T12 electron microscope.

### **AFM surface and cantilever derivatization**

AFM surface and cantilever functionalization was performed as described previously.<sup>44</sup> Prior to an experiment, AFM probes and surfaces were immersed in ~1 mL chloroform containing 20 μL of 250 mM maleimide-PEG-NHS ester (MW 3400 Da, Nanocs, NY) in DMSO and incubated at room temperature for 1 h. The PEG linkers used in this study are polydisperse with masses ±5% of the stated mass. AFM probes and surfaces were then washed with chloroform and dried with a stream of N<sub>2</sub> gas.

One hundred microliter pL constructs (50 μM in 20 mM HEPES, pH 7.5) containing engineered cysteine residues were deposited over the functionalized surface and AFM probe and left to incubate in a covered container for 30 min at room temperature. All proteins analyzed by SMFS were immobilized to functionalized probes and surfaces in the presence of 1 mM TCEP (*tris*(2-carboxyethyl)phosphine) to limit disulfide crosslinkage between proteins. Unreacted protein was then washed from the surface and AFM probe with excess reaction buffer.

### **Force spectroscopy**

All AFM measurements were conducted on an Asylum MFP-3D microscope using Si<sub>3</sub>N<sub>4</sub> cantilevers with nominal spring constants of 30 pN nm<sup>-1</sup> (Bruker MLCT). For each cantilever used, the spring constant was determined using the thermal method<sup>58</sup> using Asylum software. The approach speed was kept constant at 2 μm s<sup>-1</sup>. A retraction speed of 1 μm s<sup>-1</sup> was used for SMFS experiments that probed the dimerization of scaffolds. Typically force maps of 500 force-distance curves were taken over a 20 μm<sup>2</sup> area.

One dataset typically comprised four force maps (2000 force distance curves). All experiments were conducted in 20 mM HEPES pH 7.5 at room temperature.

All force spectroscopy data were analyzed using IGOR pro 6.32A with an Asylum Research extension (MFP3DXop v30). A force-extension profile was binned for analysis when single characteristic, parabolic WLC events were observed. For each profile, the force ( $F_R$ ) and contour length ( $L_C$ ) at rupture was measured. To obtain  $L_C$ , each force-extension profile was manually fit to a WLC model<sup>59</sup> [with a fixed persistence length of 0.4 nm, Eq. (1)].

$$F(x) = \frac{k_B T}{p} \left( 0.25 \left( 1 - \frac{x}{L_C} \right) \right)^2 - 0.25 + \frac{x}{L_C} \quad (1)$$

where  $F$  is the entropic restoring force,  $x$  is the extension,  $p$  is the persistence length,  $k_B$  is the Boltzman constant,  $T$  is the absolute temperature, and  $L_C$  is the contour length. Hit rates were calculated as the number of hits as a percentage of total approach-retract cycles. The average values over multiple experiments are quoted. The errors on hit rates are the standard deviation between experiments.

Single Gaussian distributions were fit to frequency histograms in order to determine the most probable  $F_R$  and  $L_C$  for each retraction velocity investigated. For each pulling velocity used, data were collected in triplicate (using a freshly prepared cantilever for each repeat).

To obtain a dynamic force spectrum (DFS), force-extension data were collected using retraction speeds between 200 and 5000 nms<sup>-1</sup>. To analyze these data, loading rates were calculated by fitting a WLC model to the rising edge of each unbinding profile when plotted as force versus tip-sample separation. The instantaneous gradient of this fit at rupture ( $WLC_{slope}$ ) was calculated by inserting the derived contour length and extension at rupture into a differentiated form of the same equation [Eq. (2)]. The loading rate at rupture was then obtained by multiplying this value by the retraction velocity.

$$WLC_{slope} = \frac{k_B T}{p} \left( \frac{1}{2L_c \left( 1 - \frac{x}{L_c} \right)^3} \right) + \frac{1}{L_c} \quad (2)$$

where  $p$  is the persistence length,  $L_C$  is the contour length,  $x$  is the extension,  $k_B$  is the Boltzmann constant, and  $T$  is the temperature.

The natural logarithm of the mean loading rate (Ns<sup>-1</sup>) at each velocity was plot against the mean rupture force ( $N$ ), which gives a linear relationship. The Bell-Evans model<sup>45</sup> [Eq. (3)] was rearranged to

use the gradient of the linear fit to calculate the distance from the transition state ( $x_u$ ) and the  $y$ -intercept for the off rate at zero force ( $k_{\text{off}}^{0F}$ )

$$F_R = \left( \frac{k_B T}{x_u} \right) \ln \left( \frac{r_f x_u}{k_{\text{off}}^{0F} k_B T} \right) \quad (3)$$

where  $k_B$  is the Boltzmann's constant,  $T$  is the temperature (in Kelvin),  $r_f$  is the rate at which force is loaded onto the complex or loading rate,  $x_u$  is the distance from the low energy state to the transition state and  $k_{\text{off}}^{0F}$  is the spontaneous unfolding or unbinding rate in the absence of force.

### Mass spectrometry

A Synapt HDMS quadrupole-time-of-flight mass spectrometer (Waters, Manchester, UK), equipped with a Triversa NanoMate (Advion Biosciences, Ithaca, NY) automated nano-ESI interface, was used for these analyses. The instrument has a traveling-wave IMS device situated between the quadrupole and the time-of-flight analyzers.

$\alpha$ Syn and  $\gamma$ Syn peptide samples and pL chimeric constructs (100  $\mu$ M final concentration in 100 mM ammonium acetate buffer, pH 6.8) were analyzed using positive mode nanoESI with a capillary voltage of 1.7 kV and a nitrogen nebulizing gas pressure of 0.8 psi. The following instrumental parameters were used: cone voltage 30 V; source temperature 60°C; backing pressure 3.2 mBar; ramped traveling wave height 7–20 V; traveling wave speed 300  $\text{ms}^{-1}$ ; IMS cell pressure 0.55 mBar. Data were acquired over the range  $m/z$  500–6000. Data were processed by use of MassLynx v4.1 and Driftscope v2.4 software supplied with the mass spectrometer. Mass calibration was achieved using cesium iodide solution, prepared by dissolving the compound in 50% (v/v) water/isopropanol to a concentration of 2 mg/mL.

### Circular dichroism (CD)

Far UV (190–260 nm) CD spectroscopy was performed on 50  $\mu$ M pL constructs (25 mM sodium phosphate buffer, 2 mM DTT, pH 8.0) in a 1 mm path length cuvette (Hellma) using a Chirascan<sup>TM</sup>-plus CD Spectrometer (Applied Photophysics, UK). CD spectra were acquired using a 1 nm bandwidth at room temperature, 1 s time step. Three scans were taken per sample.

For thermal denaturation experiments, a temperature gradient from 20 to 90°C in 1°C steps was performed. Protein samples were incubated for 180 s at each temperature before CD spectra were taken as above. The thermal melt data were analyzed on Photophysics Global3 software.

### Fluorescence spectroscopy

Intrinsic tryptophan emission spectra of 50  $\mu$ M pL constructs (25 mM sodium phosphate buffer, 2 mM DTT, pH 8.0) were measured on a Photon Technology International fluorometer (Ford, West Sussex, UK). Excitation and emission slit widths were set to 1 and 2 nm, respectively. Proteins were excited at 280 nm and emission spectra were recorded at 290–400 nm. Spectra were recorded of three replicates. All data were normalized to the unfolded state. The unfolded state was recorded in the same conditions as above in the presence of 8M urea.

### Acknowledgments

We thank the Wellcome Trust (grant code 094232) for the purchase of a Chiroscan CD spectrometer and the Wellcome Trust (grant code 094232) and the University of Leeds for funding the NMR instrumentation. The Synapt HDMS mass spectrometer was purchased with funds from the BBSRC (BB/E012558/1).

### Conflict of Interest

The authors declare no conflicts of interest.

### References

1. Dobson CM (2003) Protein folding and misfolding. *Nature* 426:884–890.
2. Dobson CM (2004) Principles of protein folding, misfolding and aggregation. *Semin Cell Dev Biol* 15:3–16.
3. Knowles TPJ, Vendruscolo M, Dobson CM (2014) The amyloid state and its association with protein misfolding diseases. *Nat Rev Mol Cell Biol* 15:384–396.
4. Verma M, Vats A, Taneja V (2015) Toxic species in amyloid disorders: oligomers or mature fibrils. *Ann Indian Acad Neurol* 18:138–145.
5. Cremades N, Cohen SIA, Deas E, Abramov AY, Chen AY, Orte A, Sandal M, Clarke RW, Dunne P, Aprile FA, Bertocini CW, Wood NW, Knowles TPJ, Dobson CM, Klenerman D (2012) Direct observation of the interconversion of normal and toxic forms of alpha-synuclein. *Cell* 149:1048–1059.
6. Lv ZJ, Krasnoslobodtsev AV, Zhang YL, Ysselstein D, Rochet JC, Blanchard SC, Lyubchenko YL (2015) Direct detection of alpha-synuclein dimerization dynamics: single-molecule fluorescence analysis. *Biophys J* 108:2038–2047.
7. McAllister C, Karymov MA, Kawano Y, Lushnikov AY, Mikheikin A, Uversky VN, Lyubchenko YL (2005) Protein interactions and misfolding analyzed by AFM force spectroscopy. *J Mol Biol* 354:1028–1042.
8. Sandal M, Valle F, Tessari I, Mammi S, Bergantino E, Musiani F, Brucale M, Bubacco L, Samori B (2008) Conformational equilibria in monomeric alpha-synuclein at the single-molecule level. *PLoS Biol* 6:e6–108.
9. Yu JP, Malkova S, Lyubchenko YL (2008) Alpha-synuclein misfolding: single molecule AFM force spectroscopy study. *J Mol Biol* 384:992–1001.
10. Brucale M, Sandal M, Di Maio S, Rampioni A, Tessari I, Tosatto L, Bisaglia M, Bubacco L, Samori B (2009) Pathogenic mutations shift the equilibria of alpha-

- synuclein single molecules towards structured conformers. *ChemBioChem* 10:176–183.
11. Dougan L, Li J, Badilla CL, Berne BJ, Fernandez JM (2009) Single homopolypeptide chains collapse into mechanically rigid conformations. *Proc Natl Acad Sci U S A* 106:12605–12610.
  12. Yu JP, Lyubchenko YL (2009) Early stages for Parkinson's development: alpha-synuclein misfolding and aggregation. *J Neuroimmune Pharm* 4:10–16.
  13. Kim BH, Palermo NY, Lovas S, Zaikova T, Keana JFW, Lyubchenko YL (2011) Single-molecule atomic force microscopy force spectroscopy study of amyloid beta-40 interactions. *Biochemistry* 50:5154–5162.
  14. Yu JP, Warnke J, Lyubchenko YL (2011) Nanoprobing of alpha-synuclein misfolding and aggregation with atomic force microscopy. *Nanomed Nanotech Biol Med* 7:146–152.
  15. Hervás R, Oroz J, Galera-Prat A, Goñi O, Valbuena A, Vera AM, Gómez-Sicilia A, Losada-Urzáiz F, Uversky VN, Menéndez M, Laurents DV, Bruix M, Carrión-Vázquez M (2012) Common features at the start of the neurodegeneration cascade. *PLoS Biol* 10:e1001335.
  16. Krasnoslobodtsev AV, Peng J, Asiago JM, Hindupur J, Rochet JC, Lyubchenko YL (2012) Effect of spermidine on misfolding and interactions of alpha-synuclein. *PLoS One* 7:e38099.
  17. Krasnoslobodtsev AV, Volkov IL, Asiago JM, Hindupur J, Rochet JC, Lyubchenko YL (2013) Alpha-synuclein misfolding assessed with single molecule AFM force spectroscopy: effect of pathogenic mutations. *Biochemistry* 52:7377–7386.
  18. Yu H, Liu X, Neupane K, Gupta AN, Brigley AM, Solanki A, Sosova I, Woodside MT (2012) Direct observation of multiple misfolding pathways in a single prion protein molecule. *Proc Natl Acad Sci U S A* 109:5283–5288.
  19. Lee CK, Wang YM, Huang LS, Lin SM (2007) Atomic force microscopy: determination of unbinding force, off rate and energy barrier for protein-ligand interaction. *Micron* 38:446–461.
  20. Farrance OE, Paci E, Radford SE, Brockwell DJ (2015) Extraction of accurate biomolecular parameters from single-molecule force spectroscopy experiments. *ACS Nano* 9:1315–1324.
  21. Tong ZH, Mikheikin A, Krasnoslobodtsev A, Lv ZJ, Lyubchenko YL (2013) Novel polymer linkers for single molecule AFM force spectroscopy. *Methods* 60:161–168.
  22. Lv ZJ, Roychoudhuri R, Condrón MM, Teplow DB, Lyubchenko YL (2013) Mechanism of amyloid beta-protein dimerization determined using single-molecule AFM force spectroscopy. *Sci Rep* 3:2880.
  23. Ueda K, Fukushima H, Masliah E, Xia Y, Iwai A, Yoshimoto M, Otero DAC, Kondo J, Ihara Y, Saitoh T (1993) Molecular-cloning of cDNA-encoding an unrecognized component of amyloid in Alzheimer Disease. *Proc Natl Acad Sci U S A* 90:11282–11286.
  24. Giasson BI, Murray IVJ, Trojanowski JQ, Lee VMY (2001) A hydrophobic stretch of 12 amino acid residues in the middle of alpha-synuclein is essential for filament assembly. *J Biol Chem* 276:2380–2386.
  25. Walder R, LeBlanc M-A, Van Patten WJ, Edwards DT, Greenberg JA, Adhikari A, Okoniewski SR, Sullan RMA, Rabuka D, Sousa MC, Perkins TT (2017) Rapid characterization of a mechanically labile  $\alpha$ -helical protein enabled by efficient site-specific bioconjugation. *J Am Chem Soc* 139:9867–9875.
  26. Oroz J, Hervás R, Carrion VM (2012) Unequivocal single-molecule force spectroscopy of proteins by AFM using pFS vectors. *Biophys J* 102:682–690.
  27. Krasnoslobodtsev AV, Zhang YL, Viazovkina E, Gall A, Bertagni C, Lyubchenko YL (2015) A flexible nanoarray approach for the assembly and probing of molecular complexes. *Biophys J* 108:2333–2339.
  28. Maity S, Viazovkina E, Gall A, Lyubchenko YL (2017) Single-molecule probing of amyloid nano-ensembles using the polymer nanoarray approach. *Phys Chem Chem Phys* 19:16387–16394.
  29. Vera AM, Carrión-Vázquez M (2016) Direct identification of protein-protein interactions by single-molecule force spectroscopy. *Angew Chem Intl Ed* 55:13970–13973.
  30. Tuttle MD, Comellas G, Nieuwkoop AJ, Covell DJ, Berthold DA, Kloepper KD, Courtney JM, Kim JK, Barclay AM, Kendall A, Wan W, Stubbs G, Schwitters CD, Lee VMY, George JM, Rienstra CM (2016) Solid-state NMR structure of a pathogenic fibril of full-length human alpha-synuclein. *Nat Struct Mol Biol* 23:409–415.
  31. Biere AL, Wood SJ, Wypych J, Steavenson S, Jiang YJ, Anafi D, Jacobsen FW, Jarosinski MA, Wu GM, Louis JC, Martin F, Narhi LO, Citron M (2000) Parkinson's disease-associated alpha-synuclein is more fibrillogenic than beta- and gamma-synuclein and cannot cross-seed its homologs. *J Biol Chem* 275:34574–34579.
  32. Uversky VN, Li J, Souillac P, Millett IS, Doniach S, Jakes R, Goedert M, Fink AL (2002) Biophysical properties of the synucleins and their propensities to fibrillate-inhibition of alpha-synuclein assembly by beta- and gamma-synucleins. *J Biol Chem* 277:11970–11978.
  33. Smith DP, Giles K, Bateman RH, Radford SE, Ashcroft AE (2007) Monitoring copopulated conformational states during protein folding events using electrospray ionization-ion mobility spectrometry-mass spectrometry. *J Am Soc Mass Spectrom* 18:2180–2190.
  34. Woods LA, Platt GW, Hellewell AL, Hewitt EW, Homans SW, Ashcroft AE, Radford SE (2011) Ligand binding to distinct states diverts aggregation of an amyloid-forming protein. *Nat Chem Biol* 7:730–739.
  35. Young LM, Cao P, Raleigh DP, Ashcroft AE, Radford SE (2014) Ion mobility spectrometry-mass spectrometry defines the oligomeric intermediates in amylin amyloid formation and the mode of action of inhibitors. *J Am Chem Soc* 136:660–670.
  36. Young LM, Mahood RA, Saunders JC, Tu LH, Raleigh DP, Radford SE, Ashcroft AE (2015) Insights into the consequences of co-polymerisation in the early stages of IAPP and amyloid beta peptide assembly from mass spectrometry. *Analyst* 140:6990–6999.
  37. Young LM, Saunders JC, Mahood RA, Reville CH, Foster RJ, Ashcroft AE, Radford SE (2016) ESI-IMS-MS: a method for rapid analysis of protein aggregation and its inhibition by small molecules. *Methods* 95:62–69.
  38. O'Neill JW, Kim DE, Baker D, Zhang KYJ (2001) Structures of the B1 domain of protein L from *Peptostreptococcus magnus* with a tyrosine to tryptophan substitution. *Acta Cryst D* 57:480–487.
  39. Minard P, Scalley-Kim M, Watters A, Baker D (2001) A "loop entropy reduction" phage-display selection for folded amino acid sequences. *Protein Sci* 10:129–134.
  40. Brockwell DJ, Beddard GS, Paci E, West DK, Olmsted PD, Smith DA, Radford SE (2005) Mechanically unfolding the small, topologically simple protein L. *Biophys J* 89:506–519.
  41. Sadler DP, Petrik E, Taniguchi Y, Pullen JR, Kawakami M, Radford SE, Brockwell DJ (2009)

- Identification of a mechanical rheostat in the hydrophobic core of protein L. *J Mol Biol* 393:237–248.
42. Aden J, Wittung-Stafshede P (2014) Folding of an unfolded protein by macromolecular crowding in vitro. *Biochemistry* 53:2271–2277.
  43. Marko JF, Siggia ED (1995) Stretching DNA. *Macromolecules* 28:8759–8770.
  44. Hickman SJ, Cooper REM, Bellucci L, Paci E, Brockwell DJ (2017) Gating of TonB-dependent transporters by substrate-specific forced remodelling. *Nat Commun* 8:14804.
  45. Evans E, Ritchie K (1997) Dynamic strength of molecular adhesion bonds. *Biophys J* 72:1541–1555.
  46. Evans E (2001) Probing the relation between force-lifetime and chemistry in single molecular bonds. *Annu Rev Biophys Biomol Struct* 30:105–128.
  47. Erba EB, Petosa C (2015) The emerging role of native mass spectrometry in characterizing the structure and dynamics of macromolecular complexes. *Protein Sci* 24:1176–1192.
  48. Morel B, Varela L, Azuaga AI, Conejero-Lara F (2010) Environmental conditions affect the kinetics of nucleation of amyloid fibrils and determine their morphology. *Biophys J* 99:3801–3810.
  49. Buell AK, Galvagnion C, Gaspar R, Sparr E, Vendruscolo M, Knowles TP, Linse S, Dobson CM (2014) Solution conditions determine the relative importance of nucleation and growth processes in alpha-synuclein aggregation. *Proc Natl Acad Sci U S A* 111:7671–7676.
  50. Tipping KW, Karamanos TK, Jakhria T, Iadanza MG, Goodchild SC, Tuma R, Ranson NA, Hewitt EW, Radford SE (2015) pH-induced molecular shedding drives the formation of amyloid fibril-derived oligomers. *Proc Natl Acad Sci U S A* 112:5691.
  51. Celik E, Moy VT (2012) Nonspecific interactions in AFM force spectroscopy measurements. *J Mol Recognit* 25:53–56.
  52. George JM (2002) The synucleins. *Genome Biol* 3:3002.1–3002.6.
  53. Jha NN, Ranganathan S, Kumar R, Mehra S, Panigrahi R, Navalkar A, Ghosh D, Kumar A, Padinhateeri R, Maji SK (2017) Complexation of NAC-derived peptide ligands with the C-terminus of alpha-synuclein accelerates its aggregation. *Biochemistry* 57:L791–L804.
  54. Janowska MK, Wu KP, Baum J (2015) Unveiling transient protein-protein interactions that modulate inhibition of alpha-synuclein aggregation by beta-synuclein, a pre-synaptic protein that co-localizes with alpha-synuclein. *Sci Rep* 5:15164.
  55. Bertocini CW, Fernandez CO, Griesinger C, Jovin TM, Zweckstetter M (2005) Familial mutants of alpha-synuclein with increased neurotoxicity have a destabilized conformation. *J Biol Chem* 280:30649–30652.
  56. Bertocini CW, Jung YS, Fernandez CO, Hoyer W, Griesinger C, Jovin TM, Zweckstetter M (2005) Release of long-range tertiary interactions potentiates aggregation of natively unstructured alpha-synuclein. *Proc Natl Acad Sci U S A* 102:1430–1435.
  57. Cho MK, Nodet G, Kim HY, Jensen MR, Bernado P, Fernandez CO, Becker S, Blackledge M, Zweckstetter M (2009) Structural characterization of alpha-synuclein in an aggregation prone state. *Protein Sci* 18:1840–1846.
  58. Hutter JL, Bechhoefer J (1993) Calibration of atomic-force microscope tips. *Rev Sci Instrum* 64:1868–1873.
  59. Bustamante C, Marko JF, Siggia ED, Smith S (1994) Entropic elasticity of lambda-phage DNA. *Science* 265:1599–1600.